Electronic Supplementary Material (ESI) for Energy & Environmental Science.

Supporting Information

High-throughput Computational Prediction of the Cost of Carbon Capture using Mixed Matrix Membranes

Samir Budhathoki,[a,b] Olukayode Ajayi,[a] Janice A. Steckel[a] and Christopher E. Wilmer[a,c]
[a]National Energy and Technology Laboratory, 626 Cochrans Mill Road, Pittsburgh, Pennsylvania 15236, USA
[b]AECOM, 626 Cochrans Mill Road, Pittsburgh, PA 15236, USA
[c]Department of Chemical and Petroleum Engineering, University of Pittsburgh,
3700 O'Hara St, Pittsburgh, Pennsylvania 15261, USA

[c]To whom correspondence should be addressed: e-mail wilmer@pitt.edu

S1. Widom particle insertion method

S2. Molecular dynamics (MD) simulations

S3. Polymer properties

S4. Process modelling

S1. Widom particle insertion method

Gas adsorption (CO_2, N_2) in MOFs at low partial pressures was modelled by calculating the Henry's Law constants for single-component adsorption via the Widom particle insertion method[1] as implemented in RASPA[2] at 298 K. The workflow was automated by means of python scripts. One thousand configurational-biased insertions were performed. The cutoff used for the van der Waals and electrostatic energies was 12 Å, and the Ewald summation was used to handle long range electrostatic interactions. Each simulation cell was replicated in three dimensions so as to obey the minimum image convention. For simulations in which the standard deviation of the Henry's Law constant was larger than 40%, the number of configurational-biased insertions was increased to 10,000. If the CO_2 Henry's Law constant was less than 0.001 cm^3 (STP)/cm^3 or the standard deviation of the Henry's Law constant was larger than the calculated Henry's Law constant, the MOF was removed from our material set.

S2. Molecular dynamics (MD) simulations

The molecular dynamics package LAMMPS[3] was used to compute the self-diffusivities of CO_2 and N_2 in the MOFs in the hypothetical and CoRE databases at 298 K. The cutoffs for the van der Waals and electrostatic energies and the size of the unit cell were the same as was used for the Widom particle insertion method. The initial configurations were generated using the software package PACKMOL[4] with 10 CO_2 or N_2 molecules inside the MOF framework structures, to approximate the infinite dilution condition. VMD[5] was used to generate input data files for LAMMPS. Random veolocities were assigned to the gas molecules and the system was equilibrated for 200 ps in the canonical (NVT) ensemble, in which the temperature was maintained using the Nose-Hoover thermostat[6] with a damping factor of 0.1 ps. The equilibration simulation was followed by a production run of 2 ns in the microcanonical (NVE) ensemble. A 1 fs time-step was used and velocities were recorded every 0.1 ps. Long-range electrostatics were handled using the particle-particle-particle-mesh Ewald method.[7]The self-diffusion coefficients of CO_2 and N_2 in the MOF structures were computed from the NVE trajectories using the Green-Kubo relation,[8] as shown in equation 1.

$$D = \int_0^\infty \frac{1}{\mathrm{d}N} \sum_{i=1}^{N} \langle \vec{v}_i(t).\vec{v}_i(0) \rangle dt \tag{1}$$

where $\vec{v}_i(t)$ and $\vec{v}_i(0)$ are the center of mass (COM) velocities of the adsorbates at time t and t=0, respectively, d is the dimensionality of the system, and N is the total number of adsorbates. The term in the brackets is the velocity auto correlation function (VACF). However, the VACF has noise in the long time tail, which makes integration difficult. Therefore, to predict self-diffusion coefficients, an empirical exponential decay function (equation 2) was fit to the asymptotic part of the running integral of the VACF,[9]

$$D(t) = D + a\mathrm{e}^{-bt} \tag{2}$$

where *D(t)* is the running integral in equation 1 and D, b and a are fitting parameters. The standard deviation in D was computed from the covariance matrix of the fit. As an example, the normalized VACF of CO_2 in hypothetical MOF number 3164 and 100002 are shown in Figures 1 (a) and 1 (c), and the numerical integration and exponential fit are shown in Figures 1 (b) and 1 (d). In some of the MOFs, the VACF of the gas had large oscillations or noise, possibly due to gas molecules getting caught in the cavities, and the exponential fit yielded negative values of self-diffusion coefficients. These MOFs were removed from our database. Also, the MOFs for which the self-diffusion coefficients were smaller than the uncertainties were rejected.

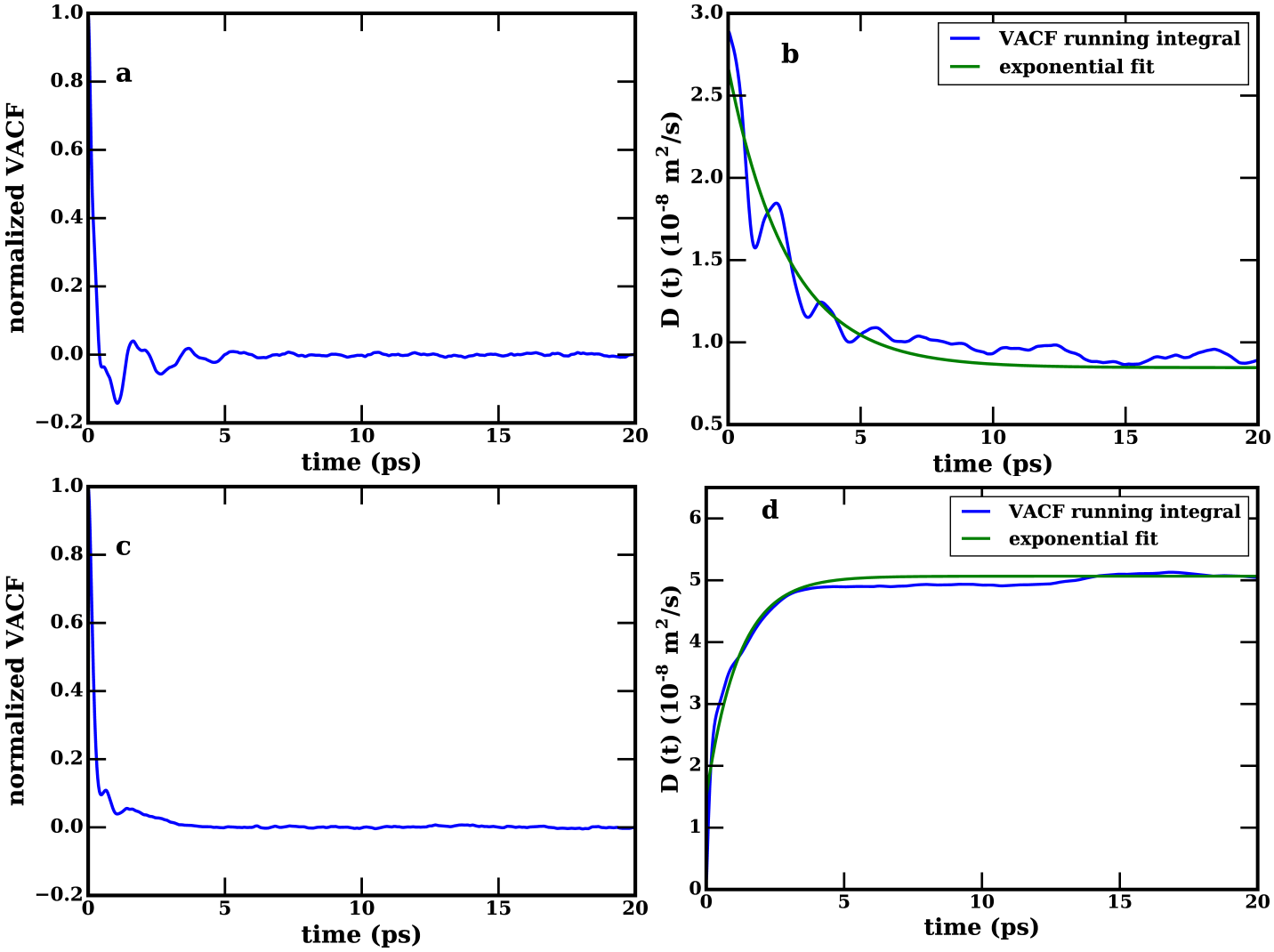

Figure 1 Normalized velocity autocorrelation function (VACF) of MOF 3164 (a) and MOF 100002 (c) and exponential fits ((b),(d)) used to calculate self-diffusivity for gases.

Nanoporous materials have pore networks that can be 1, 2 or 3 dimensional with geometric variations along different directions leading to anisotropic diffusion. For this work, we defined the diffusion of gases to be isotropic if the MOF had 3 dimensional channels, and anisotropic for MOFs with 2 or 1 dimensional channels. In making such an assumption, we have assumed that the channels in MOFs are like highways with no side streets, and no tortuosity. So, the value of d in equation 1 was assigned to be 3, 2 or 1 based on the dimensionality of channels in MOFs. Even though this is a simplified definition of diffusion anisotropy, it provides us an efficient way of estimating the self-diffusion coefficient of gases while taking diffusion anisotropy into account.

Self-diffusion coefficients of CO_2 and N_2 as a function of LCD and PLD are shown in Figure 13. It is observed that the MOFs with LCD and PLD $<$ 10 Å show larger variations in the self diffusion coefficients of both the CO_2 and N_2, ranging from zero to the maximum while MOFs with LCD or PLD $>$ 10 Å show self diffusion coefficients in excess of 10^{-9} m^2/s to the maximum. In general, the gas diffusivities of gases tend to increase increasing pore size.

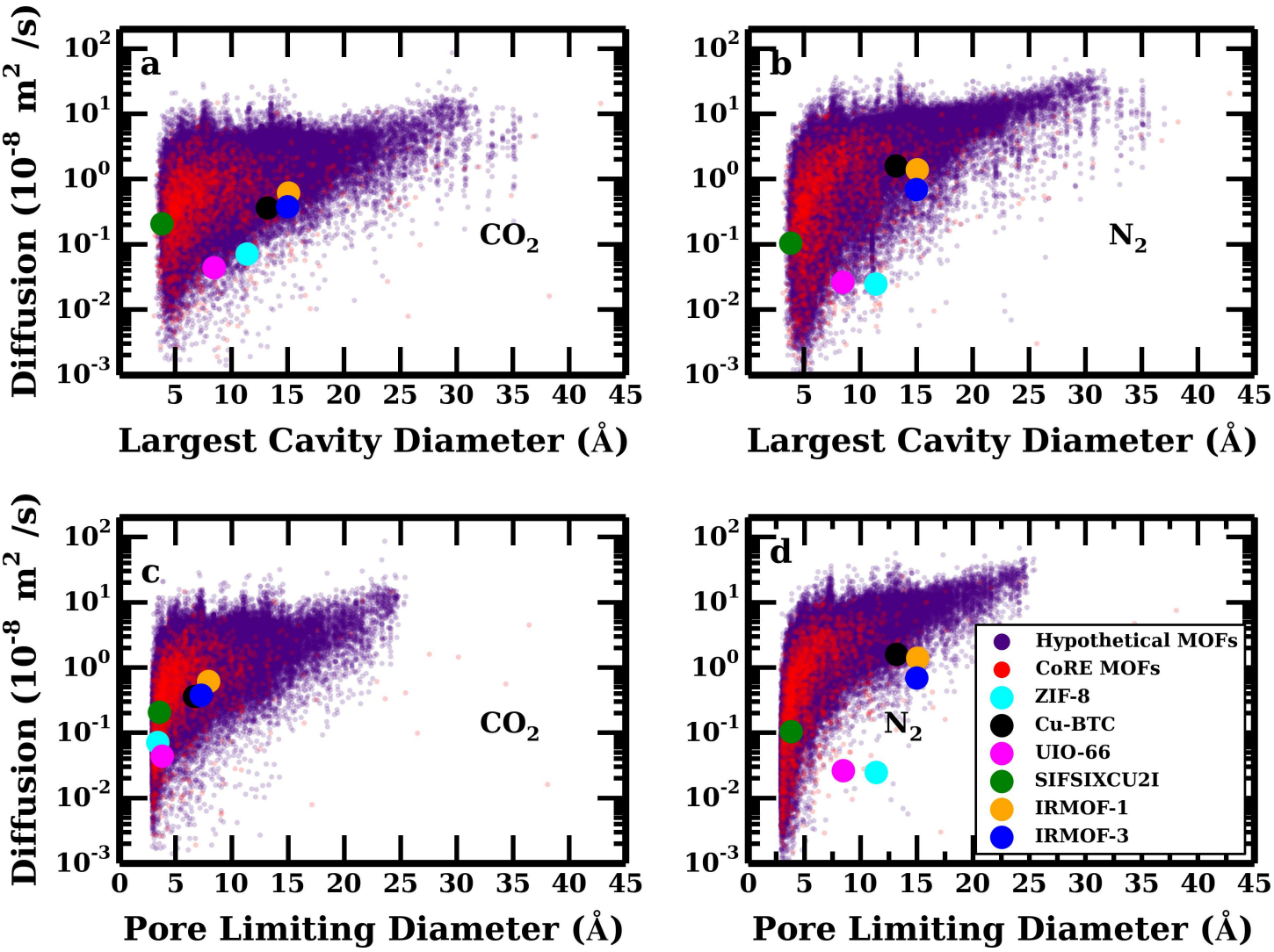

Figure 2 Self-diffusion coefficients of CO_2 and N_2 in MOFs as a function of LCD and PLD.

S3. Polymer properties

Table 1 Polymer properties

Polymer Abbv.	Full Name	CO_2/N_2 Selectivity	CO_2 Permeability (barrer)	Temp	Ref.
PTMSP	poly[1-(trimethylsilyl)-1-propyne]	10.74	29000	23 °C	10
PTMGP	poly[1-(trimethylgermyl)-1-propyne]	14	14000	23 °C	10
PIM-1	polymers of intrinsic microporosity-1	19.3	4700	40 °C	11
PDMS	polydimethylsiloxane	9.5	3800	35 °C	12
modified-PDMS	2,6-diisopropylphenyl amino-hydroxy functionalized polydimethylsiloxane	34.17	2050.4	35 °C	13
PIM-7	polymers of intrinsic microporosity-7	26.19	1100	30 °C	14
6FDA-durene	2,2'bis(3,4'-dicarboxyphenyl) hexafluoroporpane dianhydride - 2,3,5,6-tetramethyl-1,4-phenylenediamine	17.51	678	35 °C	15
MEEP	poly[bis(2-(2-methoxyethoxy)ethoxy)] polyphosphazene	62.5	250	30 °C	16
Matrimid-5218	5(6)-1-(4' aminophenyl)-1,3,-trimethylindane	8.5	29	22 °C	17

S4. Process modelling

To assess the market competitiveness of the hypothetical mixed matrix membranes (MMMs), we have conducted techno-economic analyses of potential optimized carbon capture processes based on MMMs. The goal of our process modelling was to estimate a cost of carbon capture (CCC) for any membrane based on its CO_2/N_2 selectivity and CO_2 permeance. The techno-economic evaluation was based on a CO_2 capture rate of 90%, which is the basis for the U.S. Department of Energy (DOE) carbon capture cost targets.[18] In this study, the capture process was based on a 650 MWe super critical pulverized coal power plant.[18]

The evaluation was performed making use of the three-stage membrane configuration depicted in Figure 3. This NETL-variant configuration is based on the work of Merkel et al.[19] The flue gas is sent to a compressor and then cooled to 38 degree Celsius to achieve the desired driving force and temperature prior to entering the 1^{st} stage membrane. The composition of the gas stream is given in Table 2. The retentate from the 1^{st} stage is then sent to the 2nd stage for further separation before being released. A fraction of the boiler air feed is used as sweep gas in the second membrane to increase the driving force sufficiently to remove enough CO_2 to achieve 90% capture. This sweep gas causes

some CO_2 to be recycled to the boiler, thus increasing driving force across the 2nd membrane. The oxygen depletion in the boiler is replenished by secondary air. It is essential that the model consider the impact of this larger system interaction.

Table 2 Gas stream composition

Gas	Flue gas (from Boiler) prior to compressors (mole fraction)	Inlet flue gas (1st stage) (mole fraction)	Inlet flue gas (2nd stage) (mole fraction)	Inlet flue gas (3rd stage) (mole fraction)
Ar	0.0069	0.0078	0.0087	0.0042
CO_2	0.2323	0.2625	0.1955	0.5965
H_2O	0.1544	0.0445	0.0282	0.0001
N_2	0.5716	0.6459	0.7236	0.3778
O_2	0.0348	0.0393	0.0440	0.0214

After passing through the vacuum pump, the permeate from the 1^{st} stage membrane is compressed using a multistage compressor with inter-stage cooling and sent to a liquefaction unit where it is cooled. The pressure of the resulting liquid stream (>96 mole % purity CO_2) is increased to 152 bar by a centrifugal pump to be sent via pipeline to a sequestration site. The non-condensable gas mixture from the liquefaction unit is fed to the third stage membrane. The permeate stream from the third stage is recycled to the multistage compression train, and the CO_2-depleted retentate stream is depressurized by an expander and fed into the second stage membrane.
In the Merkel configuration, the retentate from the third membrane unit is recycled to the flue gas feed. The NETL variation avoids dilution of the flue gas into the first stage, leading to an increased driving force in the first stage and a slightly lower COE.[20] Transport across the polymeric selective

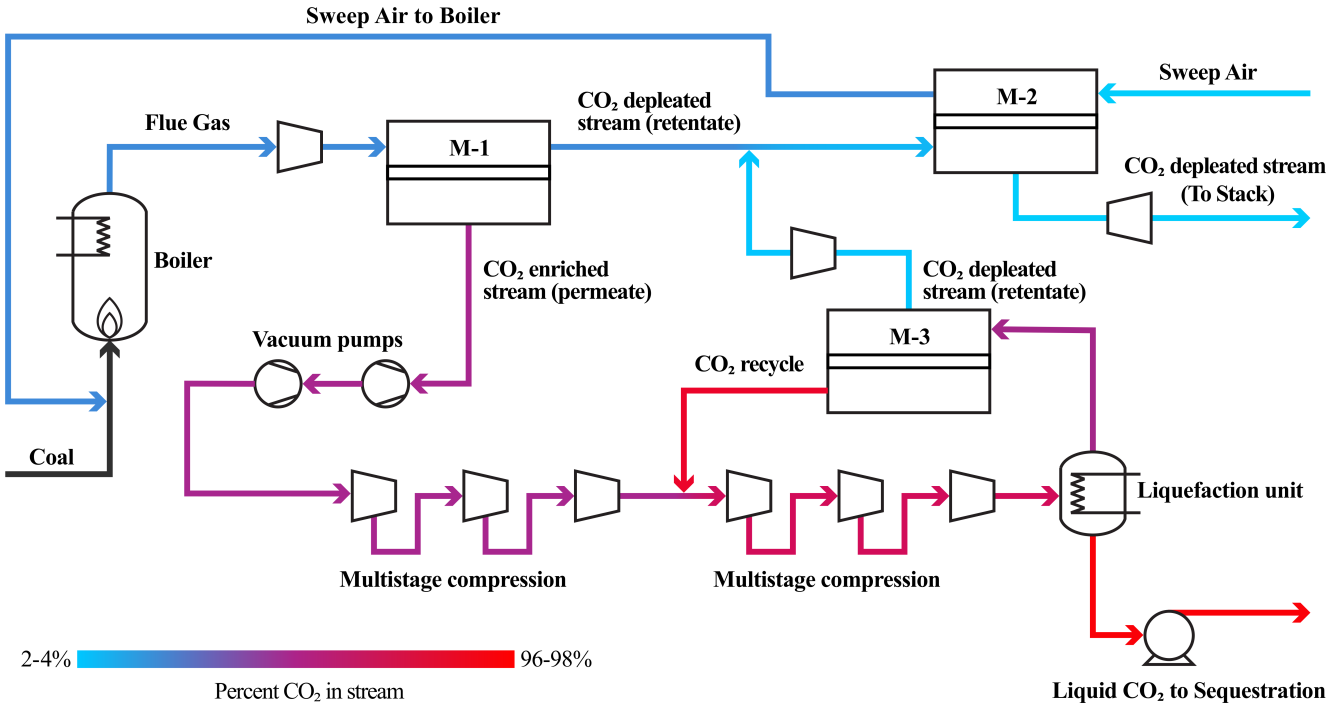

Figure 3 NETL-variant of three-stage membrane configuration initially developed by Merkel et al.[19]

layer is assumed to follow the solution-diffusion model as described by Baker.[21] An ideal CO_2 selective

membrane was modelled and the permeability of a component is the product of its solubility and diffusivity in the selective material. The driving force for gas permeation is the difference in component partial pressure across the dense skin.

$$N_i = \frac{Q_{CO_2}}{\alpha_i}\left(P_{ret}Z_{ret,i} - P_{per}Z_{per,i}\right) \tag{3}$$

where N_i, Q, α_i, P_{ret}, P_{per}, $Z_{ret,i}$, $Z_{per,i}$ are component molar flux (kmol/hr), permeance (kmol/m^{2}hrbar), membrane selectivity, pressure in the retentate (bar), permeate pressure (bar), mole fraction of gas component in shell side (kmol/kmol), and mole fraction of gas composition in fiber bore side (kmol/kmol), respectively.[22]

The total molar flux (N_t) is given by

$$N_t = \sum_i^n N_i \tag{4}$$

And the selectivity is given by

$$\alpha_i = \frac{Q_{CO_2}}{Q_i} \tag{5}$$

All the equations for the membrane module and other associated equipment such as the boiler, compressor, pumps, expanders and vacuum pumps were developed in Aspen Custom Modeler (ACM) v8.4. Properties were configured via Aspen Properties using the Peng-Robinson equation of state with the Boston-Mathias modifications (PR-BM). The cost of the membrane modules was assumed to be U.S. \$50/m^2, including the membrane, frame, valves and piping.[19,23] This cost is the same as has been adopted for previous analysis based on pure polymer membranes. The addition of MOF material would contribute very little in terms of material cost. The reason is that for a square meter of selective membrane, the selective layer is typically on the order of a micron. Thus the selective layer for one square meter amounts to about one cubic centimeter. Assuming a MOF density on the order of 1g/cm^3, it would take only 0.3 grams of MOF to make the selective layer for a MMM with 30 weight percent MOF. In a recent paper, the authors discuss large-scale MOF production and synthesis scale up, and prices on the order of \$10 to \$100 per kg of MOF are quoted.[24,25] This translates to a cost of \$0.03 per square meter of mixed matrix membrane selective layer to account for the MOF material. This argument addresses only the cost of the MOF material. It is true that the process of making a thin selective membrane out of a mixed matrix membrane rather than a neat polymer membrane might be more complicated and difficult to scale up. Recently, however, companies have created effective methods for optimizing the production of MOFs on a large scale and at lower cost.[26] The purchase costs for all the associated equipment were estimated using correlations in Seider et al.[27] A chemical engineering (CE) cost index of 527 was used in this study. The sum of all purchased costs was multiplied by a delivered cost of 1.05 and a Lang factor of 5.04 to yield total capital cost for the capture and compression system.[28] Cost correlations for all the equipment, maintenance cost and operating cost were developed within the Microsoft Excel platform.

Equation 6 was used to estimate the cost of CO_2 captured (CCC) and the reference cost of electricity (COE_{ref}) was assumed to be \$70/MWh for a power plant without carbon capture.[18] The contributions to the cost of electricity (COE) for a power plant with carbon capture (CC),[29] as shown in Equation 7, are: Total Overnight Cost (TOC_{CC}) for CC, operating variable cost ($OC_{VAF_{CC}}$) for CC and parasitic load ($MWh_{Parasitic\ load}$) due to compression work and other associated processes in the carbon capture plant. The capital cost factor (CCF) and capacity factor (CF) in Equation 7 are 0.124 and 0.85 respectively.[30] The other terms (TOC_{ref}, TOC_{FIX}, $TOC_{VAR_{ref}}$, MWh_{ref}) for the reference plant without

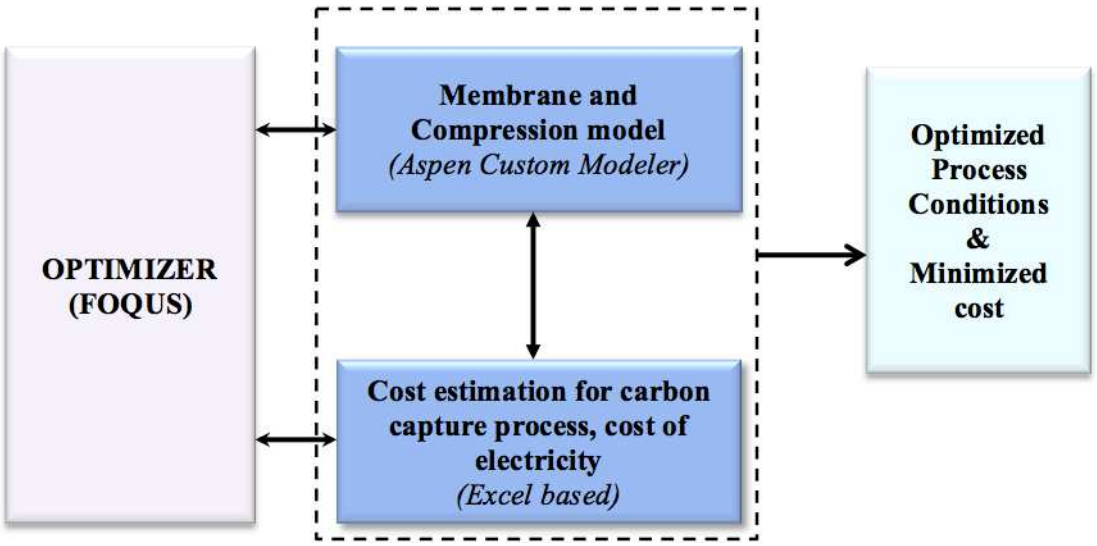

Figure 4 Methodolgy for design of CO_2 membrane processes based on techno-economic optimization.

capture are total overnight cost, fixed operating cost, variable operating cost and net power generated from power plant without carbon capture respectively.

$$CCC\ (\$/tonne_{CO_2}) = \frac{COE_{cc} - COE_{ref}}{CO_{2_{captured}}} \tag{6}$$

$$COE = \frac{(CCF)(TOC_{ref} + TOC_{cc}) + (TOC_{FIX}) + (CF)(TOC_{VAR_{ref}} + TOC_{VAR_{CC}})}{(CF)(MWh_{ref} MWh_{parasitic\ load})} \tag{7}$$

As shown in Figure 4, the techno-economic optimization was set up within Framework for Optimization, Quantification of Uncertainty and Sensitivity (FOQUS), which involves using Aspen Custom Modeler for the membrane process model and an excel-based cost estimation for the equipment cost, cost of electricity and other associated costs. A detailed description of the FOQUS software can be found in Eslick et al.[31,32] Table 3 presents the process variables subjected to optimization and the variables were constrained to certain bounds based on experience from previous runs.

Table 3 Bounded Optimization Variables

Variable	Range
Molar flow rate of sweep air into 2^{nd} stage membrane (kmol/hr)	10,000–120,000
Carbon capture fraction in 1^{st} stage membrane	0.10 – 0.9
Carbon capture fraction in 2^{nd} stage membrane	0.40 – 0.99
Carbon capture fraction in 3^{rd} stage membrane	0.50 – 0.99
Discharge pressure of the feed gas prior to 1^{st} stage membrane (bar)	1.00 – 5.00
Vacuum pressure at the permeate discharge of 1^{st} stage membrane (bar)	0.18 – 0.8
Discharge pressure of the compression train prior to liquefaction (bar)	20.0 – 35.0
Liquefaction temperature (°C)	(-35.0) – (-20.0)

The design and operating conditions of the capture process were optimized to minimize COE while maintaining 90% capture for twelve discreet simulations. Each simulation was carried out based on specific membrane properties; namely CO_2/N_2 selectivities of 18, 35, 68 or 250 and CO_2 permeances of 34, 1170 or 8000 GPU. The CO_2/Ar and CO_2/O_2 selectivity was set equal to the CO_2/N_2 selectivity and the CO_2/H_2O selectivity was set to 0.5. The cost of carbon capture for the twelve optimized systems (presented in Table 4) were used as input to develop a linear correlation to enable the rapid estimation of the cost of carbon capture as a function of CO_2 permeance and CO_2/N_2 selectivity for any arbitrary membrane. The values for permeance and selectivity were chosen such that they bound the region of interest.

Table 4 Performance Indicators for each of the 12 optimizations

CO_2 Permeance	34 GPU			
CO_2/N_2 selectivity	18	35	68	250
Compression cost ($/MWh)	60.99	51.26	47.43	43.7
Vacuum pump cost ($/MWh)	8.12	6.4	5.68	5.06
Membrane area cost ($/MWh)	237.83	231.19	226.16	223.9
Liquefaction cost ($/MWh)	3.61	3.05	2.81	2.72
Cost of Electricity (COE) (%)	385.68	359.31	346.08	336.4
Net Power Output (MWe*)	483	507	517	527
Cost of CO_2 Captured ($/ton)	243.72	238.24	233.94	231.98
CO_2 Permeance	1170 GPU			
CO_2/N_2 selectivity	18	35	68	250
Compression cost ($/MWh)	33.64	29.17	26.48	25.29
Vacuum pump cost ($/MWh)	4.46	4.24	4.04	4.33
Membrane area cost ($/MWh)	31.23	27.51	26.16	22.64
Liquefaction cost ($/MWh)	3.23	2.99	2.81	2.64
Cost of Electricity (COE) (%)	101.1	87.39	80.41	72.71
Net Power Output (MWe*)	527	541	549	556
Cost of CO_2 Captured ($/ton)	69.63	61.8	57.71	52.88
CO_2 Permeance	8000 GPU			
CO_2/N_2 selectivity	18	35	68	250
Compression cost ($/MWh)	36.34	25.06	21.55	19.2
Vacuum pump cost ($/MWh)	4.16	3.45	3.29	3.31
Membrane area cost ($/MWh)	14.55	13.96	12.98	12.44
Liquefaction cost ($/MWh)	3.59	3.03	2.87	2.5
Cost of Electricity (COE) (%)	91.24	68.11	59.18	53.06
Net Power Output (MWe*)	507	540	553	561
Cost of CO_2 Captured ($/ton)	60.47	48.1	42.78	38.92

*Gross power output of base plant is 650 MWe

References

[1] B. Widom, *J. Chem. Phys.*, 1963, **39**, 2808–2812.

[2] D. Dubbeldam, S. Calero, D. E. Ellis and R. Q. Snurr, *Molecular Simulation*, 2016, **42**, 81–101.

[3] S. Plimpton, *J. Comput. Phys.*, 1995, **117**, 1–19.

[4] L. Martínez, R. Andrade, E. G. Birgin and J. M. Martínez, *J. Comput. Chem.*, 2009, **30**, 2157–2164.

[5] W. Humphrey, A. Dalke and K. Schulten, *J. Mol. Graphics. Modell.*, 1996, **14**, 33–38.

[6] W. G. Hoover, *Phys. Rev. A*, 1985, **31**, 1695–1697.

[7] R. W. Hockney and J. W. Eastwood, *Computer Simulation Using Particles*, Taylor and Francis, Bristol, PA, 1988.

[8] M. P. Allen and D. J. Tildesley, *Computer Simulation of Liquids*, Oxford University Press, New York, 1987.

[9] C. Rey-Castro and L. F. Vega, *J. Phys. Chem. B*, 2006, **110**, 14426–14435.

[10] T. Mizumoto, T. Masuda and T. Higashimura, *J. Polym. Sci. A Polym. Chem.*, 1993, **31**, 2555–2561.

[11] A. K. Sekizkardes, V. A. Kusuma, G. Dahe, E. A. Roth, L. J. Hill, A. Marti, M. Macala, S. R. Venna and D. Hopkinson, *ChemComm.*, 2016, **52**, 11768–11771.

[12] T. C. Merkel, V. I. Bondar, K. Nagai, B. D. Freeman and I. Pinnau, *J. Polym. Sci. B Polym. Phys.*, 2000, **38**, 415–434.

[13] U. Senthilkumar and B. S. R. Reddy, *J. Membr. Sci.*, 2007, **292**, 72–79.

[14] P. M. Budd, K. J. Msayib, C. E. Tattershall, B. S. Ghanem, K. J. Reynolds, N. B. McKeown and D. Fritsch, *J. Membr. Sci.*, 2005, **251**, 263–269.

[15] W.-H. Lin and T.-S. Chung, *J. Membr. Sci.*, 2001, **186**, 183–193.

[16] C. J. Orme, M. K. Harrup, T. A. Luther, R. P. Lash, K. S. Houston, D. H. Weinkauf and F. F. Stewart, *J. Membr. Sci.*, 2001, **186**, 249–256.

[17] S. R. Venna, M. Lartey, T. Li, A. Spore, S. Kumar, H. B. Nulwala, D. R. Luebke, N. L. Rosi and E. Albenze, *J. Mater. Chem. A*, 2015, **3**, 5014–5022.

[18] M. C. Woods, P. J. Capicotto, J. L. Haslbeck, N. J. Kuehn, M. Matuszewski, L. L. Pinkerton, M. D. Rutkowski, R. L. Schoff and V. Vaysman, *Cost and Performance Baseline for Fossil Energy Plants*, DOE/NETL technical report, 2007.

[19] T. C. Merkel, H. Lin, X. Wei and R. Baker, *J. Membr. Sci.*, 2010, **359**, 126–139.

[20] O. Ajayi, *under preparation*, 2017.

[21] R. W. Baker, *Membrane technology and applications*, John Wiley & Sons, 2004.

[22] J. Morinelly and D. Miller, *Gas permeation carbon capture — Process modeling and optimization, International Pittsburgh Coal Conference*, 2011.

[23] A. Alshehri, R. Khalilpour, A. Abbas and Z. Lai, *Energy Procedia*, 2013, **37**, 976–985.

[24] D. DeSantis, J. A. Mason, B. D. James, C. Houchins, J. R. Long and M. Veenstra, *Energy Fuels*, 2017, **31**, 2024–2032.

[25] J. Liu, P. K. Thallapally, B. P. McGrail, D. R. Brown and J. Liu, *Chem. Soc. Rev.*, 2012, **41**, 2308–2322.

[26] A. Scott, *Semiconductor industry to begin using MOFs | August 7, 2017 Issue - Vol. 95 Issue 32 | Chemical & Engineering News*, `https://cen.acs.org/articles/95/i32/Semiconductor-industry-begin-using-MOFs.html`.

[27] W. D. Seider, J. D. Seader, R. D. Lewin and S. Widalgo, *Product and Process Design Principles: Synthesis, Analysis and Design*, John Wiley & Sons, Hoboken, NJ, 2009.

[28] I. AACE, *Recommended Practice No. 59R-10, Development of Factored Cost Estimates - As applied in Engineering, Procurement, And Construction for The Process Industries*, 2011.

[29] K. Gerdes, W. M. Summers and J. Wimer, *Cost Estimation Methodology for NETL Assessments of Power Plant Performance*, DOE/NETL final report, 2011.

[30] T. Fout, A. Zoelle, D. Keairns, M. Turner, M. Woods, N. Kuehn, V. Shah, V. Chou and L. Pinkerton, *Cost and Performance Baseline for Fossil Energy Plants Volume 1a: Bituminous Coal (PC) and Natural Gas to Electricity*, DOE/NETL final report, 2015.

[31] J. C. Eslick, B. Ng, Q. Gao, C. H. Tong, N. V. Sahinidis and D. C. Miller, *Energy Procedia*, 2014, **63**, 1055–1063.

[32] D. C. Miller, D. Agarwal, D. Bhattacharyya, J. Boverhof, Y. W. Cheah, Y. Chen, J. Eslick, J. Leek, J. Ma, P. Mahapatra, B. Ng, N. V. Sahinidis, C. Tong and S. E. Zitney, in *26th European Symposium on Computer Aided Process Engineering*, ed. Z. Kravanja and M. Bogataj, Elsevier, 2016, vol. 38 of Computer Aided Chemical Engineering, pp. 2391 – 2396.